

IRON IN HOT DA WHITE DWARFS

STÉPHANE VENNES¹, PIERRE CHAYER^{2,3}, JEAN DUPUIS⁴, AND THIERRY LANZ⁵

Draft version September 30, 2018

ABSTRACT

We present a study of the iron abundance pattern in hot hydrogen-rich (DA) white dwarfs. The study is based on new and archival far ultraviolet spectroscopy of a sample of white dwarfs in the temperature range $30,000\text{K} \lesssim T_{\text{eff}} \lesssim 64,000\text{K}$. The spectra obtained with the *Far Ultraviolet Spectroscopic Explorer* along with spectra obtained with the *Hubble Space Telescope* Imaging Spectrograph and the *International Ultraviolet Explorer* sample Fe III to Fe VI absorption lines enabling a detailed iron abundance analysis over a wider range of effective temperatures than previously afforded. The measurements reveal abundance variations in excess of two orders of magnitude between the highest and the lowest temperatures probed, but also show considerable variations (over one order of magnitude) between objects with similar temperatures and surface gravities. Such variations in cooler objects may be imputed to accretion from unseen companions or so-called circumstellar debris although the effect of residual mass-loss and selective radiation pressure in the hottest objects in the sample remain dominant.

Subject headings: stars: abundances — stars: atmospheres— white dwarfs

1. INTRODUCTION

The cooling history of white dwarfs involves phases of chemical transformation of their atmospheres. One such transformation occurs early on the hydrogen-rich (DA) cooling sequence. Far ultraviolet (FUV) spectroscopy of hot, hence young DA white dwarfs show that iron is a dominant source of atmospheric opacity (Vennes et al. 1992; Holberg et al. 1993). The effect of iron-group opacities has also been observed in extreme ultraviolet (EUV) spectra of the same stars as well as in other objects with similar parameters (Dupuis et al. 1995; Wolff et al. 1998; Schuh et al. 2002). Before reaching a cooling age of a few million years ($t_{\text{cool}} \leq 2 - 3 \times 10^6$ years) this source of opacity vanishes in most DA white dwarfs, and the metallicity (i.e., $n(\text{Fe})/n(\text{H})$ by number) drops from nearly solar values (Vennes & Lanz 2001) to less than $10^{-2}(Fe/H)_{\odot}$, i.e., below the detection threshold of high-dispersion *International Ultraviolet Explorer* (IUE) or even Space Telescope Imaging Spectrograph (STIS) high-resolution spectra (Barstow et al. 2003). However, the absence of an effective iron abundance diagnostics in cooler white dwarfs ($20,000\text{K} \lesssim T_{\text{eff}} \lesssim 40,000\text{K}$, or $t_{\text{cool}} = 80 - 4 \times 10^6$ years), reserved detailed iron abundance analyses to a few young objects ($t_{\text{cool}} \leq 2 - 3 \times 10^6$ years). A spectral window limited to $\lambda > 1150\text{\AA}$ restricts the iron abundance analysis to Fe IV, Fe V, and Fe VI species which are dominant in white dwarfs with $T_{\text{eff}} \gtrsim 40,000\text{K}$, and to Fe II represented by a strong doublet at $\lambda\lambda 1260.533/1267.422\text{\AA}$ and dominant in cool

white dwarfs ($T_{\text{eff}} \lesssim 20,000\text{K}$). However, in the temperature range $20,000 - 40,000\text{K}$ the ionization balance shifts toward Fe III. Spectral lines of Fe III are prominent near $\lambda \approx 1125\text{\AA}$ in a spectral window made accessible by the *Far Ultraviolet Spectroscopic Explorer* (FUSE).

The new possibilities offered by FUSE were demonstrated in a study of the DA white dwarf GD 394 ($T_{\text{eff}} \approx 37,000\text{K}$). The presence of trace elements in the otherwise hydrogen-dominated atmosphere of GD 394 had been established, among others, by Paerels & Heise (1989) in their analysis of EUV photometry of several hot white dwarfs observed with EXOSAT. The source of opacity remained uncertain (see Wolff et al. 1998; Dupuis et al. 2000) until Chayer et al. (2000) measured a surprisingly high abundance of iron in their analysis of new FUSE spectra. They used several lines of Fe III to determine an iron abundance almost solar ($Fe/H \sim 5 \times 10^{-6}$). Such a high abundance goes against the trend inferred in the study of hotter white dwarfs and indicate a resurgence of heavy elements in the atmosphere of aging DA white dwarfs. Since Chayer et al. (1995) demonstrated that the abundance of iron supported by selective radiation pressure decreases well under a solar abundance at $T_{\text{eff}} \lesssim 50,000\text{K}$, external causes are suspected, in particular accretion from the ISM, a close companion, or from a circumstellar shell.

To investigate the question further, we initiated a study of FUV spectra of a sample of twelve DA white dwarfs observed with FUSE, IUE, and STIS. The sample covers a range of effective temperatures from $\leq 64,000\text{K}$ down to $\geq 30,000\text{K}$. We describe the sample selection process in §2, with relevant EUV/soft X-ray data listed in Appendix A, and we present the FUV observations in §3. The model atmospheres and spectral synthesis used in this investigation are presented in §4, and our analysis is presented in §5. Finally, we summarize and discuss our results in §6.

2. SAMPLE SELECTION: SERENDIPITOUS AND

DELIBERATE

¹ Department of Physics and Space Sciences, Florida Institute of Technology, 150 W University Blvd., Melbourne, FL 32901-6975

² Department of Physics and Astronomy, Johns Hopkins University, 3400 N. Charles St., Baltimore, MD 21218-2686

³ Also at Department of Physics and Astronomy, University of Victoria, P.O. Box 3055, Station Csc, Victoria, BC V8W 3P6, Canada.

⁴ Canadian Space Agency, 6767 route de l'Aéroport, Saint-Hubert, QC J3Y 8Y9, Canada.

⁵ Department of Astronomy, University of Maryland, College Park, MD 20742.

Electronic address: svennes@fit.edu, chayer@pha.jhu.edu, Jean.Dupuis@space.gc.ca, tlanz@umd.edu.

We searched for high-metallicity white dwarfs in the sample collected as part of the *FUSE* Z903 and P204 programs (Dupuis et al. 2005; Vennes et al. 2005). The programs assembled over 40 DA white dwarfs selected for observations on the basis of their predicted UV luminosity and high equatorial latitude. The sample presents opportunities for the serendipitous identification of high metallicity DA white dwarfs. Next, we included three stars with large iron abundances initially studied by Holberg et al. (1993) and more recently by Barstow et al. (2003).

In a systematic effort to identify high-metallicity white dwarfs, we have also examined the EUV/soft X-ray properties of a large sample of 178 DA white dwarfs with effective temperatures ranging from 84,000 K down to 24,000 K, i.e., with corresponding ages ranging from 0.5 to 30 million years. The sample comprises isolated white dwarfs (Vennes et al. 1996, 1997; Vennes 1999; Vennes et al. 2006) and in binaries with luminous companions (Vennes et al. 1998). Among these, some 104 objects are joint detections from the *EUVE*/100Å survey and the *ROSAT* PSPC survey (Bowyer et al. 1996; Voges et al. 1999).

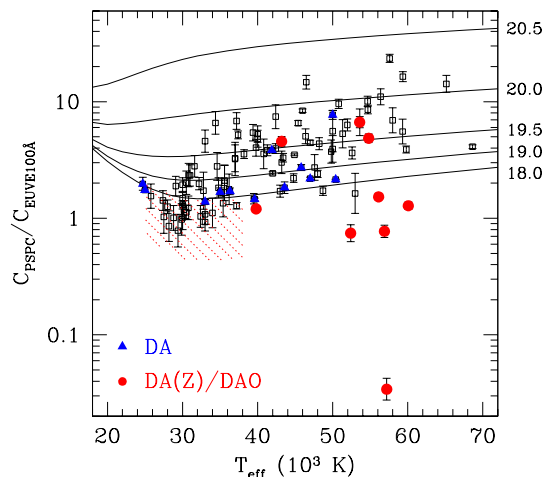


FIG. 1.— Ratio of observed *ROSAT*/PSPC to *EUVE*/100Å count rates as a function of effective temperatures for a sample of 104 objects. The data are compared to pure-H model predictions with varying ISM column densities (full lines) at $\log n_H = 18, 18.5, 19, 19.5, 20, 20.5$. Note the spectroscopically confirmed pure-H (blue triangles) and high-metallicity stars (red circles).

Figure 1 shows the *ROSAT*/PSPC to *EUVE*/100Å count rate ratio as a function of effective temperatures for spectroscopically-confirmed pure-H white dwarfs (blue triangles), and spectroscopically-confirmed high-metallicity DA/DAO white dwarfs (red circles). The remaining stars are shown with open black squares. The PSPC soft X-ray measurements probe the high-energy tail of a hot white dwarf soft X-ray emission ($\lambda \lesssim 100\text{\AA}$), and the *EUVE*/100Å measurements probe somewhat longer wavelength emission. The data, available in Appendix A are compared to predictions from pure-hydrogen models at $\log g = 8$ and varying intervening ISM column density expressed in number of neutral hydrogen atoms per cm^2 (full lines at $\log n_H =$

18, 19, 19.5, 20, 20.5). The minimum flux ratio expected from a pure-H atmosphere quickly converges to values independent of the ISM column density as it approaches $\log n_H \approx 18$. Values observed below the curve labelled $\log n_H = 18$ are incompatible with pure hydrogen atmospheres and correspond to stars contaminated with heavy elements, possibly iron. Note that the effect of increased metallicity opposes the effect of increased ISM column density, therefore the method will select in preference objects with high metallicity and low neutral hydrogen column density in the ISM. The behavior of the count rate ratio for the sub-sample of pure-H white dwarfs — among these are Sirius B, GD 71, and HZ 43—and in particular near the temperature of 30,000K, guarantees that the procedure is well calibrated. Note that surface gravity variations are imperceptible.

The red-hatched area encloses a particularly interesting sample of objects, and, immediately to the right of this area, the red circle represents the high-metallicity DA GD 394. The grouping of stars found within the red-hatched area close to the high-metallicity white dwarf GD 394 suggests possible spectroscopic similarities between these objects.

Therefore, to demonstrate that iron opacities are responsible, at least in part, for the anomalous flux ratios, we searched bright candidates with count rate ratios significantly below the minimum threshold. The DA white dwarfs GD 683 and LB 1663 (Vennes et al. 1996) stood out with PSPC to *EUVE* 100Å flux ratios of ~ 0.98 and ~ 0.93 , respectively. These ratios are inferior to the ratio measured in GD 394 (~ 1.20) and indicate the likely presence of heavy elements. These two objects have been observed as part of the *FUSE* D023 observing program.

3. FUV SPECTROSCOPY

Table 1 lists the sample of white dwarfs observed spectroscopically with *FUSE*. The observations were made using the $30 \times 30''$ low-resolution slit (LWRS) resulting in 100% throughput and insuring complete spectral coverage ($900 \lesssim \lambda \lesssim 1180\text{\AA}$) with a spectroscopic resolving power $R = \lambda/\Delta\lambda = 20000 \pm 2000$. The stars 0549+158 (GD 71), 1819+580 (*EUVE* J1820+58.0, RE J1820+580) and 2000–561 (*EUVE* J2004–56.0, RE J2004–560) were selected from the Z903 and P204 programs, and the stars GD 683 and LB 1663 were observed as part of the D023 program. We also re-analyzed the *FUSE* spectra of the DA white dwarf GD 394 (Chayer et al. 2000). All data were processed with the *FUSE* data reduction pipeline CALFUSE version 3.0. Figure 2 shows Fe III line identifications in *FUSE* spectra along with P V and Si IV line identifications.

3.1. STIS and IUE Observations

We obtained a series of STIS spectra of the hot white dwarf WD0556–375 (*EUVE* J0558–37.5, RE J0558–376) from the Multi-Mission Archive at the Space Telescope (MAST, Table 2). The spectra were obtained in the $0.2 \times 0.2''$ aperture and using the E140M grating resulting in a resolving power of $R \sim 40000$. We also obtained a series of *IUE* high-dispersion spectra of the hot DA white dwarfs WD0621–376 (*EUVE* J0623–37.6, RE J0623–374) and WD2211–495 (*EUVE* J2214–49.3, RE J2214–492) from

TABLE 1
FUSE OBSERVATIONS

| WD name | other name | 1RXS J | T_{eff} (K) | $\log g$ | V (mag) ^a | Data ID | t_{exp} (s) | Aperture |
|----------|-------------------|-----------------|--------------------|-------------------|----------------------|----------|---------------|----------|
| 0106–358 | GD 683, EUVE, RE | 010821.4–353433 | 29000 ± 600^b | 7.99 ± 0.25^b | 14.70 | D0230101 | 30835 | LWRS |
| 0320–539 | LB 1663, EUVE, RE | 032215.5–534515 | 32880 ± 1070^b | 7.98 ± 0.16^b | 14.90 | D0230201 | 9062 | LWRS |
| 0549+158 | GD 71, EUVE, RE | 055228.1+155313 | 33000 ± 300^c | 7.87 ± 0.15^c | 13.03 | P2041701 | 13929 | LWRS |
| 1819+580 | EUVE, RE | 182030.0+580437 | 44200 ± 700^c | 8.61 ± 0.21^c | 13.95 | Z9032801 | 4698 | LWRS |
| 2000–561 | EUVE, RE | 200425.2–560301 | 42200 ± 200^c | 7.84 ± 0.18^c | 14.97 | Z9033301 | 11596 | LWRS |
| 2111+498 | GD 394, EUVE, RE | 211244.1+500616 | 36700 ± 400^c | 8.27 ± 0.12^c | 13.08 | P1043601 | 28635 | LWRS |

^aFrom McCook & Sion (1999) and references therein.

^bThis work.

^cFrom Vennes et al. (2005).

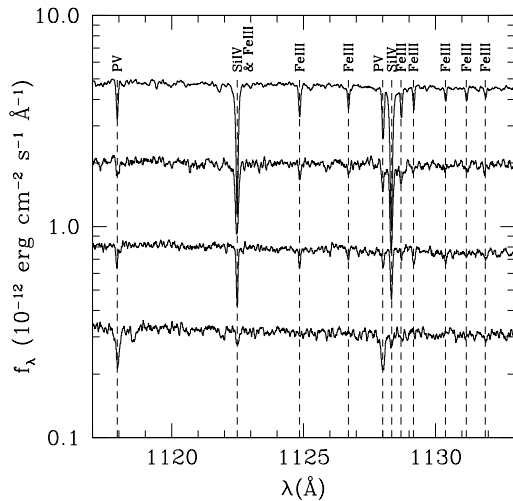


FIG. 2.— *FUSE* spectra showing iron line identifications in, from top to bottom, GD 394, WD 1819+580, GD 683, and WD 2000–561 (offset by -0.3 dex). The iron line identifications in WD J2000–561 are uncertain. The spectra also show silicon and phosphorus lines.

 TABLE 2
 STIS AND *IUE* OBSERVATIONS

| WD name | Data ID | t_{exp} (s) |
|----------|-------------------------|---------------|
| 0556–375 | O59P03010 | 2494 |
| | O59P03020 | 2977 |
| | O59P03030 | 2977 |
| 0621–376 | SWP45951HL ^a | 14400 |
| | SWP49037HL | 13800 |
| | SWP49038HL | 12600 |
| | SWP49039HL | 12600 |
| 2211–495 | SWP44766HL | 7200 |
| | SWP44767HL | 7200 |
| | SWP47954HL | 7200 |
| | SWP47955HL | 7200 |
| | SWP47956HL | 7200 |
| | SWP47996HL | 7200 |

^aSWP=short wavelength primary; HL = high dispersion large aperture.

dispersion mode and the large aperture resulting in a resolving power $R \sim 10000$ and a wavelength coverage of $1150 \lesssim \lambda \lesssim 1950 \text{ \AA}$. We co-added the spectra for each star.

4. MODEL ATMOSPHERES AND SPECTRA

The model atmospheres and synthetic spectra were calculated assuming non-local thermodynamic (non-LTE) equilibrium using the fortran codes TLUSTY version 200 and SYNSPEC version 48 (Hubeny & Lanz 1995). Using these codes, Vennes et al. (2005) computed a grid of pure hydrogen model atmospheres covering the range of effective temperatures from $T_{eff} = 20,000 \text{ K}$ to $80,000 \text{ K}$ and surface gravities from $\log g = 6.8$ to 9.6 . By comparing a grid computed assuming local thermodynamic equilibrium (LTE) to the non-LTE grid, Vennes et al. (2005) demonstrated that non-LTE effects in the Lyman line spectra of DA white dwarfs are for the most part negligible. On the other hand, Vennes et al. (2005) also studied the effect of heavy element opacities on the Lyman and Balmer line spectra of high-metallicity white dwarfs such as G191-B2B and O621–376. They demonstrated that the observed abundance of heavy elements in the photospheres of these stars accounts for discrepancies noted in effective temperatures and surface gravities measured with Balmer line spectra versus the same parameters measured with Lyman line spectra. The models assume homogeneous distribution of heavy elements over the surface, and as a function of depth in the atmosphere. Note that Schuh et al. (2002) explicitly considered a vertical distribution of heavy elements in diffusive equilibrium. A basic feature of their ab initio calculations is that stars with similar effective temperatures and surface gravities ought to display similar abundance patterns. This is not always the case as we shall demonstrate in §5, and equilibrium scenarios may easily be disrupted by accretion from a companion or even a weak wind.

Based on these considerations, we created three sets of models for the purpose of (1) analyzing the Lyman line spectra of cooler objects (GD 71, GD 683, LB 1663, 1819+580, 2000–561, and GD 394), (2) measuring the trace element abundances in the same objects, and, finally, (3) measuring the abundance of trace elements in the high-metallicity DA white dwarfs 0621–376, 2211–495, and 0556–375.

To analyze the Lyman line spectra obtained with *FUSE* (Table 1) we adopted the LTE model grid of

MAST (Table 2). The spectra were obtained in the high-

Vennes et al. (2005). The Lyman line profiles are computed using the tables of Lemke (1997). Next, having obtained the temperature and surface gravity of each star, we computed sets of three non-LTE models for each star with model atoms from the OSTAR2002 series (Lanz & Hubeny 2003). The stellar temperatures within this particular group range from $\approx 30,000$ to $\approx 45,000\text{K}$, therefore we include the ions H I (9 levels), H II, C II (22 levels), C III (23 levels), C IV (25 levels), C V (1 level), Si III (30 levels), Si IV (23 levels), Si V (1 level), P IV (14 levels), P V (17 levels), P VI (1 level), Fe II (36 super-levels), Fe III (50 super-levels), Fe IV (43 super-levels), Fe V (42 super-levels), and Fe VI (1 level). Super-levels group together levels with the same basic configuration. Figure 3 shows the equivalent widths of selected iron lines as a function of effective temperatures for abundances of $\log \text{Fe}/\text{H} = -5.3, -6.0,$ and -6.7 . The resonance lines of Fe III are dominant at effective temperatures $T_{\text{eff}} \lesssim 40,000\text{K}$.

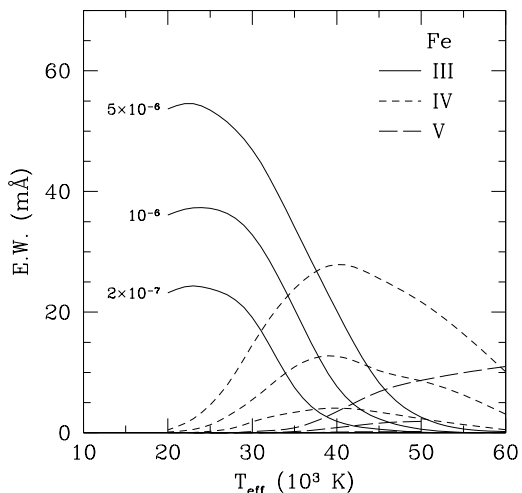


FIG. 3.— Equivalent widths of Fe III λ 1124.881, Fe IV λ 1542.698, and Fe V λ 1376.337 as a function of effective temperatures. Fe III λ 1124.881 is an excellent iron abundance diagnostics for temperatures below 30,000K, and the line remains detectable up to a temperature of $\approx 45,000\text{K}$.

Next, we extended the sequence of models presented by Vennes & Lanz (2001) in their study of Feige 24 and G191-B2B to higher abundances and temperatures encompassing likely parameters for the hot, high-metallicity DA white dwarfs 0556–375, 0621–376, and 2211–495. Three new models at $T_{\text{eff}} = 57, 60, 64 \times 10^3\text{K}$ and $\log g = 7.5$ share a high heavy-element concentration of $\log \text{He}/\text{H} = -5.0$, $\log \text{C}/\text{H} = -6.0$, $\log \text{N}/\text{H} = -5.8$, $\log \text{O}/\text{H} = -5.0$, $\log \text{Si}/\text{H} = -5.4$, $\log \text{S}/\text{H} = -5.0$, $\log \text{Fe}/\text{H} = -4.0$, and $\log \text{Ni}/\text{H} = -4.8$, while three other models at $T_{\text{eff}} = 57, 60, 64 \times 10^3\text{K}$ ($\log g = 7.5$) share a lower concentration used by Vennes & Lanz (2001). Together, these six new models cover the range of abundances and effective temperatures appropriate for an abundance study of 0556–375, 0621–376 and 2211–495.

5. ANALYSIS AND RESULTS

We assembled twelve stars with temperatures ranging from $\approx 30,000$ to $\approx 64,000\text{K}$ and we determined the

abundance of iron in their photospheres. Two stars were observed with *IUE* (0621–376 and 2211–495) while another was observed with *STIS*, and six stars were observed with *FUSE* (Table 1). To this sample we added published iron abundance analyses of the hot DA white dwarfs Feige 24, G191-B2B, and GD 246. Incidentally, we also measured abundances of carbon, silicon and phosphorous in the sample of stars observed with *FUSE*; these specific results will be discussed at a later time.

5.1. Feige 24, G191-B2B, and GD 246

In the cases of Feige 24 and G191-B2B, we adopted the abundance analysis of Vennes & Lanz (2001). Their analysis is based on the same generation of iron-rich models used in the present study. The iron equivalent widths in Feige 24 and G191-B2B are very similar and the iron abundances in these two stars are very close. For example, the Fe IV λ 1542.698 equivalent width is 11 mÅ in both objects, and the Fe V λ 1370.337 equivalent width in Feige 24 and G191-B2B is 26 and 22 mÅ, respectively. We adopted temperatures of $T_{\text{eff}} = 57,000\text{K}$ and $55,000\text{K}$ for Feige 24 and G191-B2B, respectively, as estimated by Vennes & Lanz (2001). The corresponding iron abundances are $\log \text{Fe}/\text{H} = -5.5$ and -5.6 for Feige 24 and G191-B2B, respectively. In the case of GD 246 we adopted the analysis of a *Chandra* Low Energy Transmission Grating (Vennes & Dupuis 2002). The abundance analysis of GD 246 was based on the detection of Fe V, Fe VI and Fe VII lines and resulted in an iron abundance estimate of $\log \text{Fe}/\text{H} \approx -6.5$ and $T_{\text{eff}} = 54,000\text{K}$.

5.2. Analysis of STIS and IUE Spectroscopy

Figure 4 shows the iron abundance analysis of the *FUV* spectra of the hot DA white dwarfs 0556–375, 0621–376, and 2211–495. We applied a χ^2 minimization technique to determine the abundances and 1σ errors. The analysis is restricted to a few well defined spectral lines with accurate $\log gf$.

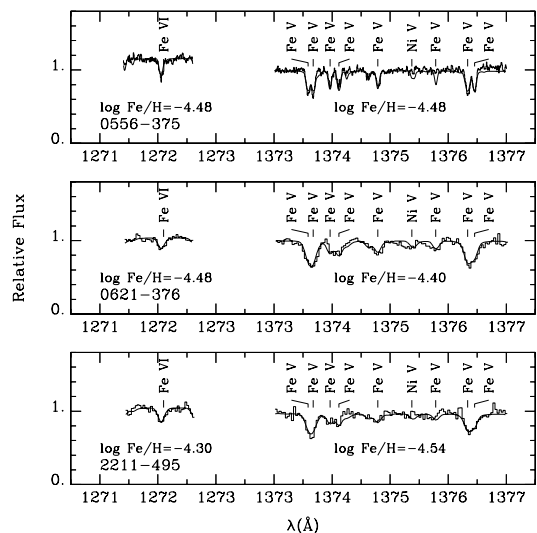


FIG. 4.— *IUE* ultraviolet spectra of WD0621–376 and WD2211–495 ($R \approx 10,000$), and *STIS* spectrum ($R \approx 40,000$) of WD0556–375, and best Fe V and Fe VI line profile fits.

We adopted effective temperatures deduced from the Balmer and Lyman line analysis of Vennes et al. (2005).

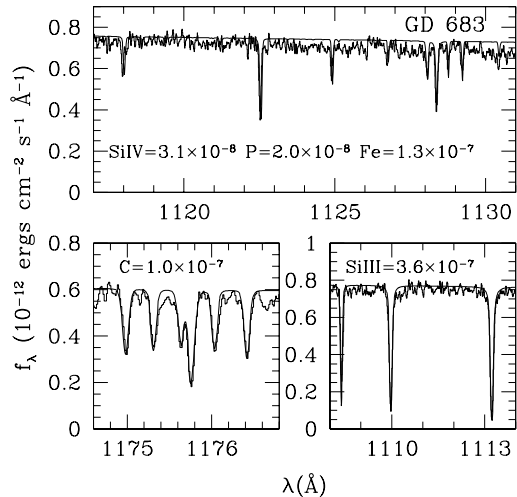


FIG. 5.— Ultraviolet spectrum of GD 683 and best C III, Si III, Si IV, P V, and Fe III line profile fits.

Vennes et al. (2005) measured the effect of metallicity using non-LTE model atmospheres and deduced effective temperatures of $T_{\text{eff}} = 60,000\text{K}$ and $62,000\text{K}$ for 0621–376 and 2211–495, respectively. Adopting the model grid of Vennes et al. (2005), we repeated the Balmer line analysis of 0556–375 (Vennes et al. 1997) and measured $T_{\text{eff}} = 68800 \pm 1000\text{K}$ and $\log g = 7.56 \pm 0.05$. The DA white dwarf 0556–375 is hotter than 2211–495 by $\approx 2800\text{K}$ and is hotter than 0621–376 by $\approx 4000\text{K}$. Again, using non-LTE metallicity vectors calculated by Vennes et al. (2005), we adopted a temperature of $T_{\text{eff}} = 64000\text{K}$ for 0556–375. Hence, the iron abundances based on FUV spectra are $\log \text{Fe}/\text{H} = -4.44 \pm 0.10$, -4.42 ± 0.10 , and -4.48 ± 0.10 for 0621–376, 2211–495, and 0556–375, respectively. The abundances based on Fe V lines are consistent with abundances based on Fe VI lines which implies that models calculated at the adopted stellar parameters predict the ionization balance correctly.

5.3. Analysis of *FUSE* Spectroscopy

Again, the analysis is restricted to a few well defined spectral lines with accurate $\log gf$. The wavelength range covering the C III line profile fits is $1174 \leq \lambda \leq 1177$ with the continuum measured on each side. Similarly the wavelength ranges covering the Fe III, P V, Si III, and Si IV are $1124 \leq \lambda \leq 1127.5$, $1117 \leq \lambda \leq 1119$, $1108 \leq \lambda \leq 1114$, and $1122 \leq \lambda \leq 1123\text{\AA}$, respectively. We applied a χ^2 minimization technique to determine the abundances and 1σ errors, or, when appropriate, the abundance upper limits. Table 3 summarizes our *FUSE* abundance analysis. Figure 5 shows the results of the analysis for the DA white dwarf GD 683. The intrinsic strengths of the Fe III lines are sufficient to allow abundance measurements ≈ 1.5 dex lower than in the extreme case of GD 394.

The ionization balance of silicon is problematic in all stars. The abundances based on Si III lines are between 0.7 and 1.0 dex larger than abundances based on Si IV lines in the same stars. The causes of this ionization im-

balance, already noted by Dupuis et al. (2000) in the case of GD 394, remain unknown. The present abundance measurements of 1819+580 and 2000–561 are somewhat at variance with those reported by Dupuis et al. (2005) which is in part due to the more comprehensive atmospheric compositions used in the present study, and, in the the case of 1819+580 to the use of atmospheric parameters determined using the Lyman line series rather than the Balmer line series.

5.4. The Iron Abundance Pattern

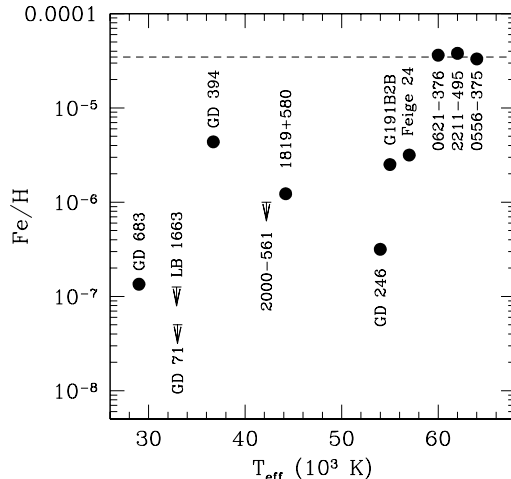


FIG. 6.— Iron abundance in a sample of DA white dwarfs observed with *HST* (G191-B2B and Feige 24), *FUSE* (GD 71, GD 683, LB 1663, GD 394, 2000–561, and 1819+580), *IUE* (0621–376 and 2211–495), *Chandra* (GD 246), and *STIS* (0556–375). The horizontal dashed line shows the solar abundance.

Figure 6 shows the iron abundance measurements in our white dwarf selection as a function of effective temperatures. The white dwarfs GD 683 and LB 1663 are closely matched in effective temperatures, but a poorer signal-to-noise ratio in the latter only allowed to establish an upper limit to the iron abundance. Although the abundances of carbon, silicon and phosphorous are markedly lower in LB 1663, the presence of iron at a comparable level than in GD 683 cannot be excluded and its presumed effect on the EUV/soft X-ray emission of LB 1663 remains a likely explanation for the anomalous PSPC/*EUVE* 100\AA flux ratio which prompted its selection. On the other hand, stringent abundance upper limits were established in the case of bright DA white dwarf GD 71 showing that objects with similar effective temperatures and surface gravities, such as GD 71 and GD 683, may have dissimilar abundance patterns. The DA GD 71 is among those objects, depicted in Figure 1, that are characterized by a very low metallicity.

The white dwarfs 1819+580 and 2000–560 are similarly paired and again a poorer signal-to-noise ratio in the latter does not permit to determine the iron abundance. However, the two stars show similar levels of carbon, silicon, and phosphorous. Clearly, 2000–561 should be re-observed with *FUSE* for a longer exposure time increasing the prospect of detecting iron in its photosphere.

Our non-LTE analysis of GD 394 confirms the results

TABLE 3
ABUNDANCES BASED ON *FUSE* SPECTROSCOPY

| WD name | C/H | Si/H | | P/H | Fe/H |
|----------|------------------|------------------|------------------|------------------|------------------|
| | | (III) | (IV) | | |
| 0106–358 | -7.00 ± 0.07 | -6.44 ± 0.06 | -7.51 ± 0.17 | -7.69 ± 0.17 | -6.87 ± 0.19 |
| 0320–539 | < -8.4 | < -8.7 | < -8.3 | < -8.7 | < -6.9 |
| 0549+158 | < -8.9 | < -9.0 | < -9.0 | -8.7 ± 0.2^a | < -7.3 |
| 1819+580 | -7.24 ± 0.07 | -7.71 ± 0.08 | -8.44 ± 0.11 | -7.64 ± 0.25 | -5.91 ± 0.29 |
| 2000–561 | -7.76 ± 0.06 | -7.50 ± 0.07 | -8.54 ± 0.10 | -7.84 ± 0.14 | < -6.0 |
| 2111+498 | < -8.8 | -5.67 ± 0.04 | -6.38 ± 0.07 | -8.00 ± 0.08 | -5.36 ± 0.09 |

^aDobbie et al. (2005) reported the detection of a weak P $\lambda 1118\text{\AA}$ line in GD 71 and measured $\log P/H = -8.6$ in agreement with our measurement.

obtained from the LTE analysis of Chayer et al. (2000). In fact, the abundance of iron in the photosphere of GD 394 exceeds that of G191-B2B and Feige 24. The hottest, hence youngest DA white dwarfs in the sample also display the highest, almost precisely solar iron abundance.

Figure 6 demonstrates the chemical transformation occurring early on ($t_{\text{cool}} \lesssim 3 \times 10^6$ years) along the DA white dwarf cooling sequence. However, the obvious resurgence of iron in the photospheres of some objects characterized by temperatures $T_{\text{eff}} \lesssim 45,000$ K is puzzling. Clearly, equilibrium diffusion calculations (Chayer et al. 1995) do not explain this behavior, and contributions from iron reservoirs external to the stars may be required.

6. DISCUSSION AND SUMMARY

We have presented a study of the iron abundance pattern in hot DA white dwarfs. We reported the discovery of Fe III spectral lines in a *FUSE* spectrum of the DA white dwarf GD 683 and a corresponding abundance $\log \text{Fe}/\text{H} = -6.9$. The discovery of iron in the photosphere of this star confirms our suspicion that heavy elements, and iron in particular, are responsible for lingering EUV/soft X-ray flux deficit in DA white dwarfs with temperatures as low as $\approx 30,000\text{K}$. The detection of iron in the DA white dwarf 1819+580 is particularly intriguing. Green et al. (2000) uncovered substantial near infrared excess from this star which they attributed to a dM6 companion, but there is insufficient information to establish its proximity to the white dwarf.

In fact, with the exception of Feige 24 and 1819+580 we do not find clear evidence of an infrared flux excess in any of the sample stars. We obtained JHK photometry from the 2MASS database available at the Centre de Donnees astronomique de Strasburg and V magnitudes from McCook & Sion (1999), and we computed $V - J$ indices for all objects in the sample. The index ranges from $V - J = -0.72 \pm 0.10$ (GD 683) to -0.96 ± 0.15 (2000–561) with the exception of 1819+580 ($V - J = -0.11 \pm 0.10$) and Feige 24 ($V - J = 1.15 \pm 0.10$). Synthetic $V - J$ indices for DA white dwarfs range from -0.7 to -0.8 for white dwarf effective temperatures between $30,000\text{K}$ and $50,000\text{K}$. Allowing for large uncertainties in 2MASS measurements, it appears that only 1819+580 and Feige 24 show evidence of a companion in infrared measurements. The estimated absolute J magnitudes

are $M_J = 11.43$ and 7.06 corresponding to M8.5 and M2.5 spectral types (Kirkpatrick & McCarthy 1994) for 1819+580 and Feige 24, respectively. The spectral type of the companion of 1819+580 is somewhat later than estimated by Green et al. (2000) because we adopted a higher gravity, hence lower luminosity, for the white dwarf itself. From our sample, only Feige 24 has a known *close* companion ($P = 4.2$ days), but its abundance pattern is indistinguishable from its sibling and apparently single white dwarf G191-B2B (Vennes & Lanz 2001). In all other cases, predicted 3σ upper limits to the companion absolute J magnitude range from $M_J \lesssim 10.3$ or a spectral type earlier than M6 (Kirkpatrick & McCarthy 1994) to $M_J \lesssim 13.3$ or a spectral type earlier than L5 (Kirkpatrick 2005). These hypothetical stellar and substellar companions may be responsible for the presence of iron in white dwarfs such as GD 683 and GD 394. Moreover, the variable EUV emission from GD 394 may imply that iron, silicon and other elements are not uniformly distributed over the surface, which may be the result of episodic accretion from a putative companion (Dupuis et al. 2000).

The iron abundance in DA white dwarfs with temperatures between $\approx 30,000$ and $\approx 64,000\text{K}$ does not correlate with effective temperatures in a simple manner. The sample of DA white dwarfs is part of a EUV/soft X-ray selected population and may be biased against ultra-high metallicity objects, although the largest iron abundance measured is essentially solar. Other non-EUV selected white dwarfs were included in a study by Barstow et al. (2003) such as PG 0948+534, Ton 21, and PG 1342+444 which, although hotter than stars from the present study, may have lower iron abundances. Other EUV-selected DA white dwarfs such as 1RXS J0619.1–0828 (Vennes 1999) lack FUV data required for an abundance analysis. Hopefully future missions may help enlarge this sample of hot DA white dwarfs.

In summary, our measurements reveal abundance variations in excess of two orders of magnitude between the highest and the lowest temperatures probed, but also show considerable variations (over one order of magnitude) between objects with similar temperatures and surface gravities. Such variations in cooler objects may be imputed to accretion from unseen companions or so-called circumstellar debris (Kilic et al. 2005) although the effect of residual mass-loss and selective radiation

pressure in the hottest objects in the sample may remain dominant. Accretion from a close companion remain a likely source of heavy elements in white dwarf photospheres. A deeper search for infrared excess, revealing the presence of a companion or debris near the white dwarf, may offer clues as to the source of iron in hot DA photospheres.

Guided by present and previous results we will embark on a re-analysis of the complete spectral energy distribution of all hot DA white dwarfs lifting the often convenient but possibly inappropriate assumption of a pure hydrogen composition. In particular, the present analysis of Fe III spectral lines, and its sensitive iron abundance diagnostics, will be extended to the complete *FUSE* spectroscopic data set.

We acknowledge support from a NASA LTSA grant

(NAG5-11844) and a *FUSE* GI grant (NNG04GF05G). This research also received financial support from the College of Science of the Florida Institute of Technology. P.C. is a Canadian representative to the *FUSE* Project supported by CSA under a PWGSC contract. We thank A. Kawka for supplying infrared colors, and the referee J. Holberg for useful comments.

This research has made use of the Simbad database and the VizieR service, operated at CDS, Strasbourg, France. This publication makes use of data products from the Two Micron All Sky Survey, which is a joint project of the University of Massachusetts and the Infrared Processing and Analysis Center, funded by the National Aeronautics and Space Administration and the National Science Foundation.

REFERENCES

- Barstow M. A., Good S. A., Holberg J. B., Hubeny I., Bannister N. P., Bruhweiler F. C., Burleigh M. R. & Napiwotzki R. 2003, *MNRAS*, 341, 870
- Bowyer, S., Lampton, M., Lewis, J., Wu, X., Jelinsky, P., & Malina, R.F. 1996, *ApJS*, 102, 129
- Chayer P., Fontaine G., & Wesemael F. 1995, *ApJS*, 99, 189
- Chayer P., Kruk J. W., Ake T. B., Dupree A. K., Malina R. F., Siegmund O. H. W., Sonneborn G., & Ohl R. G. 2000, *ApJ*, 538, L91
- Dobbie, P. D., Barstow, M. A., Hubeny, I., Holberg, J. B., Burleigh, M. R., & Forbes, A. E. 2005, *MNRAS*, 363, 763
- Dupuis, J., Chayer, P., Vennes, S., Christian, D. J., & Kruk, J. W. 2000, *ApJ*, 537, 977
- Dupuis, J., Chayer, P., Vennes, S., Kruk, J. W., Torres, L. M., & Sánchez, P. J. 2005, *ASP Conf. Ser. 334: 14th European Workshop on White Dwarfs*, 334, 191
- Dupuis, J., Vennes, S., Bowyer, S., Pradhan, A. K., & Thejll, P. 1995, *ApJ*, 455, 574
- Green, P. J., Ali, B., & Napiwotzki, R. 2000, *ApJ*, 540, 992
- Heber, U., Bade, N., Jordan, S., & Voges, W. 1993, *A&A*, 267, L31
- Holberg, J. B., et al. 1993, *ApJ*, 416, 806
- Hubeny, I., & Lanz, T. 1995, *ApJ*, 439, 875
- Kilic, M., von Hippel, T., Leggett, S. K., & Winget, D. E. 2005, *ApJ*, 632, L115
- Kirkpatrick, J. D. 2005, *ARA&A*, 43, 195
- Kirkpatrick, J. D., & McCarthy, D. W., Jr. 1994, *AJ*, 107, 333
- Lanz, T., & Hubeny, I. 2003, *ApJS*, 146, 417
- Lemke, M. 1997, *A&A*, 122, 285
- McCook, G. P., & Sion, E. M. 1999, *ApJS*, 121, 1
- Paerels, F.B.S., Heise, J. 1989, *ApJ*, 339, 1000
- Schuh S. L., Dreizler S. & Wolff B. 2002, *A&A*, 382, 164
- Vennes, S. 1999, *ApJ*, 525, 995
- Vennes, S., Chayer, P., Thorstensen, J. R., Bowyer, S., & Shipman, H. L. 1992, *ApJ*, 392, L27
- Vennes, S., Chayer, P., Dupuis, J., & Lanz, T. 2005, *ASP Conf. Ser. 334: 14th European Workshop on White Dwarfs*, 334, 185
- Vennes, S., Christian, D.J., & Thorstensen, J.R. 1998, *ApJ*, 502, 763
- Vennes, S., & Dupuis, J. 2002, *ASP Conf. Ser. 262: The High Energy Universe at Sharp Focus: Chandra Science*, 262, 57
- Vennes, S., Dupuis, J., Kawka, A. 2006, in preparation
- Vennes, S., & Lanz, T. 2001, *ApJ*, 553, 399
- Vennes, S., Thejll, P. A., Wickramasinghe, D. T., & Bessell, M. S. 1996, *ApJ*, 467, 782
- Vennes, S., Thejll, P., Genova-Galvan, R., & Dupuis, J. 1997, *ApJ*, 480, 714
- Voges, W., et al. 1999, *A&A*, 349, 339
- Wolff, B., Koester, D., Dreizler, S., & Haas, S. 1998, *A&A*, 329, 1045

APPENDIX

SOFT X-RAY TO EUV COUNT RATE RATIOS

Table A4 lists the PSPC to *EUVE* 100Å count rate ratios for a sample of 104 hot DA white dwarfs detected in both surveys (Bowyer et al. 1996; Voges et al. 1999). The stars are listed with the PSPC catalog designation, and temperature estimates are provided in references cited in §2, except for 1RXS J082704.9+284411 which is taken from Heber et al. (1993). These temperature estimates are used in the selection process depicted in Figure 1 only. Many have been updated since.

TABLE A4
SOFT X-RAY TO EUV COUNT RATE RATIOS

| <i>ROSAT</i> name | $C_{\text{PSPC}}/C_{100\text{\AA}}$ | T_{eff} (10^3K) | <i>ROSAT</i> name | $C_{\text{PSPC}}/C_{100\text{\AA}}$ | T_{eff} (10^3K) |
|-----------------------|-------------------------------------|--|-----------------------|-------------------------------------|--|
| 1RXS J000359.1+433600 | 7.44± 1.72 | 42.4 | 1RXS J103347.4-114146 | 1.55± 0.37 | 25.8 |
| 1RXS J000732.4+331730 | 9.58± 0.87 | 50.8 | 1RXS J103624.9+460838 | 1.19± 0.21 | 30.2 |
| 1RXS J002958.0-632500 | 3.89± 0.27 | 59.8 | 1RXS J104311.5+490227 | 2.40± 0.17 | 48.0 |
| 1RXS J005317.6-325951 | 1.71± 0.11 | 36.3 | 1RXS J104446.6+574449 | 2.35± 0.53 | 30.8 |
| 1RXS J010821.4-353433 | 0.98± 0.29 | 29.9 | 1RXS J105820.6-384416 | 0.85± 0.25 | 28.2 |
| 1RXS J013424.0-160708 | 1.72± 0.16 | 48.7 | 1RXS J105916.6+512452 | 4.11± 0.15 | 68.6 |
| 1RXS J013853.1+252325 | 5.43± 0.88 | 39.4 | 1RXS J110036.4+713758 | 1.71± 0.20 | 43.0 |
| 1RXS J015109.6+673947 | 2.33± 0.48 | 31.0 | 1RXS J111140.4-224933 | 1.48± 0.17 | 30.0 |
| 1RXS J022818.9-611817 | 4.44± 0.22 | 47.0 | 1RXS J111238.8+240909 | 4.03± 0.66 | 39.8 |
| 1RXS J023725.5-122129 | 1.04± 0.22 | 32.4 | 1RXS J112619.1+183925 | 0.77± 0.09 | 56.9 |
| 1RXS J023947.9+500349 | 2.79± 0.75 | 34.6 | 1RXS J114804.5+183042 | 1.03± 0.32 | 27.5 |
| 1RXS J030437.1+025706 | 2.02± 0.68 | 35.6 | 1RXS J120055.5-363013 | 3.23± 1.03 | 37.0 |
| 1RXS J031713.9-853231 | 1.94± 0.26 | 30.0 | 1RXS J123645.3+475530 | 1.53± 0.08 | 56.1 |
| 1RXS J032215.5-534515 | 0.93± 0.16 | 33.0 | 1RXS J125702.4+220155 | 1.45± 0.04 | 39.6 |
| 1RXS J033714.6-415541 | 5.58± 2.16 | 50.0 | 1RXS J131621.4+290555 | 2.15± 0.01 | 50.4 |
| 1RXS J034850.1-005823 | 4.57± 0.44 | 43.2 | 1RXS J144006.0+750539 | 3.96± 0.37 | 42.4 |
| 1RXS J035629.1-364134 | 3.94± 1.01 | 50.0 | 1RXS J144602.4+632929 | 3.56± 1.02 | 40.8 |
| 1RXS J042734.0+740735 | 10.07± 1.01 | 54.7 | 1RXS J150021.1+745838 | 5.55± 1.33 | 59.3 |
| 1RXS J044307.1-034655 | 14.22± 2.34 | 65.1 | 1RXS J152944.2+483623 | 2.73± 0.67 | 47.6 |
| 1RXS J045712.5-280754 | 0.03± 0.01 | 57.2 | 1RXS J153545.2-772439 | 6.93± 1.67 | 58.0 |
| 1RXS J051206.1-004149 | 1.98± 0.24 | 32.2 | 1RXS J162334.0-391359 | 1.97± 0.25 | 24.7 |
| 1RXS J051223.5-414525 | 3.63± 0.43 | 52.6 | 1RXS J162909.4+780439 | 3.50± 0.06 | 44.9 |
| 1RXS J051523.8+324107 | 2.43± 0.08 | 42.0 | 1RXS J163825.8+350006 | 6.83± 1.11 | 37.2 |
| 1RXS J052119.2-102925 | 1.08± 0.21 | 33.0 | 1RXS J165851.0+341852 | 5.31± 1.44 | 51.3 |
| 1RXS J055038.1+000553 | 5.05± 0.74 | 46.4 | 1RXS J165948.2+440059 | 1.13± 0.15 | 30.5 |
| 1RXS J055047.4-240853 | 6.66± 1.72 | 53.6 | 1RXS J171127.2+664532 | 14.69± 1.95 | 46.5 |
| 1RXS J055228.1+155313 | 1.39± 0.06 | 33.0 | 1RXS J172642.8+583726 | 23.53± 1.85 | 57.6 |
| 1RXS J060502.5-481944 | 2.11± 0.61 | 35.6 | 1RXS J172738.9-360015 | 1.72± 0.60 | 32.8 |
| 1RXS J063258.1-050547 | 3.30± 0.28 | 43.4 | 1RXS J174614.9-703902 | 3.83± 0.41 | 41.3 |
| 1RXS J063350.3+104122 | 1.42± 0.27 | 27.4 | 1RXS J180009.9+683557 | 8.37± 0.27 | 46.0 |
| 1RXS J064509.3-164241 | 1.74± 0.04 | 25.0 | 1RXS J182030.0+580437 | 6.55± 0.33 | 45.4 |
| 1RXS J064855.3-252350 | 1.26± 0.16 | 28.0 | 1RXS J184509.8+682239 | 5.19± 0.41 | 37.4 |
| 1RXS J065414.2-020940 | 1.11± 0.32 | 34.0 | 1RXS J184739.3+015732 | 1.30± 0.10 | 30.0 |
| 1RXS J071506.6-702540 | 1.83± 0.21 | 43.6 | 1RXS J184756.1-221938 | 2.79± 0.59 | 31.6 |
| 1RXS J072047.8-314705 | 0.74± 0.12 | 52.4 | 1RXS J191824.6+595953 | 4.59± 1.00 | 33.0 |
| 1RXS J072320.0-274720 | 1.28± 0.08 | 37.2 | 1RXS J192558.3-563344 | 7.71± 0.69 | 50.0 |
| 1RXS J072905.9-384839 | 5.27± 0.85 | 40.0 | 1RXS J194343.1+500440 | 6.57± 1.45 | 34.4 |
| 1RXS J080933.1-725909 | 1.23± 0.28 | 30.8 | 1RXS J200905.6-602537 | 3.84± 0.11 | 41.9 |
| 1RXS J082335.2-252522 | 3.02± 0.66 | 43.2 | 1RXS J201310.0+400222 | 6.67± 0.74 | 53.6 |
| 1RXS J082704.9+284411 | 4.81± 0.80 | 40.0 | 1RXS J202400.4-422429 | 1.89± 0.36 | 29.1 |
| 1RXS J083151.0-534029 | 2.02± 0.46 | 30.5 | 1RXS J211244.1+500616 | 1.20± 0.06 | 39.8 |
| 1RXS J084104.2+032118 | 3.55± 0.31 | 38.2 | 1RXS J211652.9+735037 | 8.56± 0.71 | 54.7 |
| 1RXS J084548.9+485241 | 1.47± 0.15 | 39.5 | 1RXS J212458.2+282553 | 1.63± 0.62 | 53.0 |
| 1RXS J091422.0+021916 | 1.01± 0.23 | 30.0 | 1RXS J212626.8+192224 | 1.68± 0.13 | 35.0 |
| 1RXS J091657.6-194613 | 11.03± 1.73 | 56.4 | 1RXS J212743.5-221145 | 3.73± 0.84 | 49.8 |
| 1RXS J094021.7+502116 | 1.77± 0.52 | 36.2 | 1RXS J215453.3-302935 | 0.78± 0.24 | 29.4 |
| 1RXS J095752.3+852935 | 6.32± 0.74 | 52.0 | 1RXS J215621.5-543820 | 2.72± 0.16 | 45.8 |
| 1RXS J101628.3-052026 | 4.85± 0.41 | 54.8 | 1RXS J215635.1-414220 | 4.36± 0.51 | 48.2 |
| 1RXS J102405.9+262113 | 3.27± 0.85 | 37.0 | 1RXS J221030.3-300546 | 1.01± 0.24 | 28.8 |
| 1RXS J102444.5-302102 | 1.83± 0.36 | 34.8 | 1RXS J224952.6+583430 | 16.40± 1.61 | 59.4 |
| 1RXS J102945.3+450717 | 1.34± 0.35 | 35.4 | 1RXS J231221.6+104657 | 1.28± 0.09 | 60.1 |
| 1RXS J103210.2+532941 | 2.18± 0.06 | 47.0 | 1RXS J232431.0-544148 | 2.21± 0.19 | 44.8 |